Multi-layer hydraulic exchange flows

By G. F. LANE-SERFF[1]†, D. A. SMEED[2]
AND C. R. POSTLETHWAITE[1]

[1]School of Ocean and Earth Science
[2]James Rennell Division,
University of Southampton, Southampton Oceanography Centre, Southampton SO14 3ZH, UK

Flows between ocean basins are often controlled by narrow channels and shallow sills. A multi-layer hydraulic control theory is developed for exchange flow through such constrictions. The theory is based on the inviscid shallow-water equations and extends the functional approach introduced by Gill (1977) and developed by Dalziel (1991). The flows considered are those in rectangular–cross-section channels connecting two large reservoirs, with a single constriction (sill and/or narrows). The exchange flow depends on the stratification in the two reservoirs, represented as a finite number of immiscible layers of (different) uniform density. For most cases the flow is 'controlled' at the constriction and often at other points along the channel (virtual controls) too. As with one- and two-layer hydraulics, controls are locations at which the flow passes from one solution branch to another, and at which (at least) one internal wave mode is stationary. The theory is applied to three-layer flows, which have two internal wave modes, predicting interface heights and layer fluxes from the given reservoir conditions. The theoretical results for three-layer flows are compared to a comprehensive set of laboratory experiments and found to give good agreement. The laboratory experiments also show other features of the flow, such as the formation of waves on the interfaces. The implications of the results for oceanographic flows and ocean modelling are discussed.

1. Introduction

The large-scale thermohaline ocean circulation, especially the flow of dense deep waters, is often restricted by topography with flow limited to gaps where straits and sills may induce hydraulic control. The exchanges between semi-enclosed marginal seas and the global ocean are also determined by flows through straits as well as the processes occurring within the enclosed basins. Motivated by these geophysical flows a number of authors have used hydraulic models, which are based on the shallow water equations, to study the idealized problem of the exchange between two reservoirs of a two-layer stratified fluid. Initial studies examined steady inviscid flows through channels with rectangular cross-section, see for example Wood (1970), Armi (1986), Armi & Farmer (1986), Farmer & Armi (1986) and Dalziel (1991). Subsequently these models have been extended to include other effects, such as non-rectangular cross-section (e.g. Bormans & Garrett 1989; Dalziel 1992*a*), rotation (e.g. Dalziel 1990; Pratt & Lundberg 1991), dissipation (e.g. Bormans & Garrett 1989) and time-dependent forcing (e.g. Helfrich 1995).

† Present address: Department of Civil and Structural Engineering, UMIST, PO Box 88, Manchester, M60 1QD, UK.
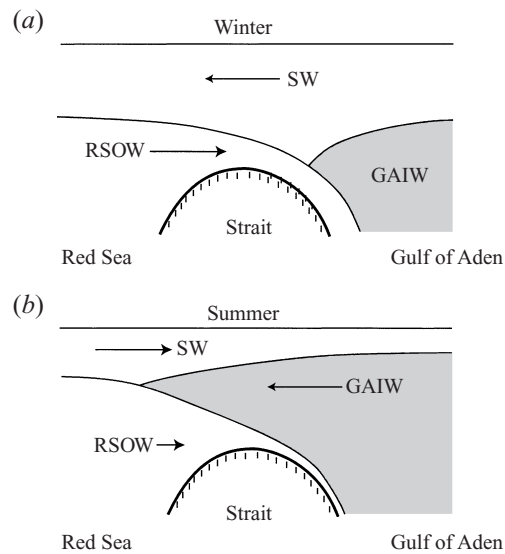
FIGURE 1. Schematic showing the flow through Bab al Mandab at the mouth of the Red Sea during (*a*) the winter monsoon, (*b*) the summer monsoon. Note the change in the thickness of the surface water (SW) in the Gulf of Aden, the change in direction of flow of this water and the arresting of the inflow of Gulf of Aden Intermediate Water (GAIW) during the winter. The flow of Red Sea Overflow Water (RSOW) is greatest during the winter.

Two-layer models have given much insight to oceanic flows, such as that through the Strait of Gibraltar (Farmer & Armi 1988; Bryden & Kinder 1991; Bryden *et al.* 1994). However, to obtain a complete understanding of these flows it is necessary to consider more general stratification. Furthermore, there are some flows which cannot be represented by two-layer exchange. For example, the flow through Bab al Mandab, which connects the Red Sea to the Gulf of Aden, has three distinct water masses (Smeed 1997; Murray & Johns 1997; Pratt *et al.* 1999). During the summer monsoon water flows out of the Red Sea both at the surface and at depth, with an inflow of intermediate water between the outflowing layers. During the winter monsoon surface water flows into the Red Sea (figure 1), while dense Red Sea Overflow Water (RSOW) continues to flow out. Thus we need a three-layer hydraulic theory to describe the flow at the mouth of the Red Sea.

There has been relatively little work on hydraulic control with more complicated stratification. Killworth (1992) examined the conditions for hydraulic control in a continuously stratified fluid. A number of authors have considered related flows, including stratified flow over an obstacle (Baines 1987, 1988, 1995; Denton 1990), or withdrawal of fluid from a stratified reservoir by a localized sink (e.g. Benjamin 1981; Imberger & Patterson 1989; Armi & Williams 1993). These problems are also examined in the book by Baines (1995). In all of these cases the flow is forced, uni-directional flow. Here we consider the flow that is driven by stratification in essentially static reservoirs at each end of a connecting channel.

Recently Smeed (2000) has outlined a three-layer hydraulic theory, and used it to explain the observations of flow in the Bab al Mandab. The work is developed further in this paper in which a wider class of three-layer exchange flows is considered and the results are compared with a series of laboratory experiments. The theory is
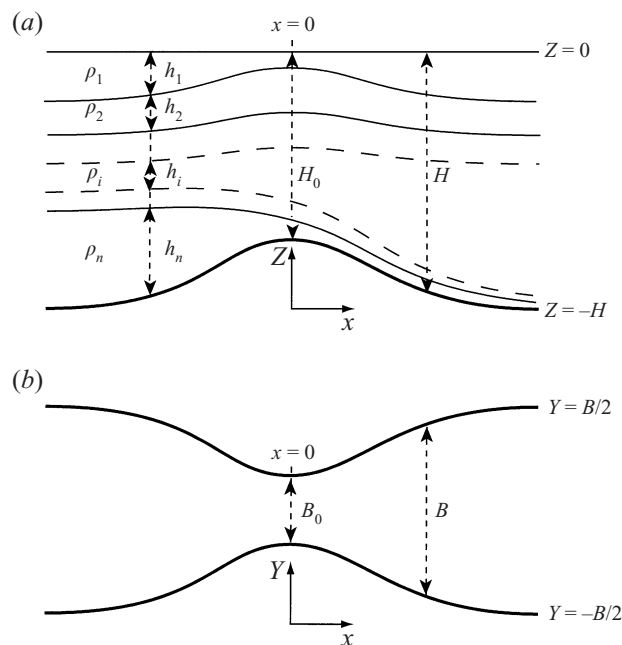
FIGURE 2. Multi-layer flow along a channel, showing the notation used in the multi-layer model.

also extended to consider an arbitrary number of layers and the implications for continuously stratified flows are discussed.

The development of the hydraulic theory is given in §2, and follows the functional approach introduced by Gill (1977) and developed by Dalziel (1991). Some results of the theory for a three-layer flow with a contraction† are given in §3. The laboratory experiments are described in §4 with the results given in §5. The theoretical and laboratory results are discussed and compared in §6 and the work is summarized and some conclusions drawn in §7.

2. Multi-layer hydraulic control theory

2.1. *Flow configuration and equations for multi-layer flow*

The problem considered is one in which two large reservoirs are connected by a channel of rectangular cross-section. The width and depth of the channel vary on scales long compared to the channel length so that the fluid velocity has a significant component in the along-channel, x-direction, only. The fluid consists of a number (n) of immiscible layers of (different) uniform density, $\rho_i, i = 1, \ldots, n$. We assume that the flow is Boussinesq, hydrostatic and inviscid. The layer thicknesses are denoted by h_i and velocities in each layer by u_i. The u_i may be positive or negative, with the direction of flow in each layer depending on external conditions. The flow and parameters are illustrated in figure 2.

There is a rigid lid and the total depth of the channel is $H(x) = h_1 + h_2 + \cdots + h_n$,

---

† We use the term 'constriction' to refer to a general minimum in the cross-sectional size of the channel, while a 'contraction' refers to a minimum in the width of a channel of constant depth.

while the width is denoted by $B(x)$. Continuity gives

$$\frac{\partial a_i}{\partial t} + \frac{\partial}{\partial x}(u_i a_i) = 0, \quad i = 1,\ldots,n, \tag{1}$$

where $a_i = B h_i$ is the cross-sectional area of each layer.

The reduced gravity across each interface is denoted by $g_i' = g(\rho_{i+1} - \rho_i)/\bar{\rho}$, $i = 1,\ldots,(n-1)$ and $\bar{\rho}$ is the mean density. The momentum equations for each layer are

$$\frac{\partial u_1}{\partial t} + \frac{\partial}{\partial x}\left(\tfrac{1}{2}u_1^2 + \frac{p_0}{\bar{\rho}}\right) = 0, \tag{2.1}$$

$$\frac{\partial u_2}{\partial t} + \frac{\partial}{\partial x}\left(\tfrac{1}{2}u_2^2 + \frac{p_0}{\bar{\rho}} - g_1' h_1\right) = 0, \tag{2.2}$$

$$\frac{\partial u_3}{\partial t} + \frac{\partial}{\partial x}\left(\tfrac{1}{2}u_3^2 + \frac{p_0}{\bar{\rho}} - g_1' h_1 - g_2'(h_1 + h_2)\right) = 0, \tag{2.3}$$

$$\vdots$$

$$\frac{\partial u_n}{\partial t} + \frac{\partial}{\partial x}\left(\tfrac{1}{2}u_n^2 + \frac{p_0}{\bar{\rho}} - g_1' h_1 - g_2'(h_1 + h_2) - \cdots - g_{n-1}'(h_1 + h_2 + \cdots + h_{n-1})\right) = 0, \tag{2.n}$$

where p_0 is the pressure at $z = 0$.

For steady flow, the continuity equations (1) imply that the flux in each layer is constant,

$$u_i a_i = Q_i, \quad i = 1,\ldots,n, \tag{3}$$

Bernoulli equations are obtained by integrating the difference between equations (2.1) and (2.2), between (2.2) and (2.3),..., (2.n–1) and (2.n) to give $(n-1)$ equations,

$$\tfrac{1}{2}u_1^2 - \tfrac{1}{2}u_2^2 + g_1' h_1 = H_1', \tag{4.1}$$

$$\tfrac{1}{2}u_2^2 - \tfrac{1}{2}u_3^2 + g_2'(h_1 + h_2) = H_2', \tag{4.2}$$

$$\vdots$$

$$\tfrac{1}{2}u_{n-1}^2 - \tfrac{1}{2}u_n^2 + g_{n-1}'(h_1 + h_2 + \cdots + h_{n-1}) = H_{n-1}', \tag{4.n–1}$$

where $H_1' \ldots H_{n-1}'$ are constants.

The equations are non-dimensionalized using the minimum values of the channel depth and width, H_0 and B_0, and the total reduced gravity, $g' = g_1' + g_2' + \cdots + g_{n-1}'$, as follows:

$$\left.\begin{array}{c} B = B_0 b, \quad H = H_0 h, \quad g_i' = r_i g', \quad i = 1,\ldots,(n-1), \\[4pt] h_i = H_0 h y_i, \quad i = 1 \ldots n, \\[4pt] H_i' = g' H_0 H_i, \quad i = 1,\ldots,(n-1), \quad Q_i = B_0 H_0 (g' H_0)^{1/2} q_i, \quad i = 1,\ldots,n. \end{array}\right\} \tag{5}$$

Thus $h(x)$ and $b(x)$ are the non-dimensional depth and width of the channel (with $h(x) \geqslant 1$, $b(x) \geqslant 1$). The non-dimensional depths of the layers are $y_i(x)$, with $y_1 + \cdots + y_n = 1$. The parameters $r_i = (\rho_{i+1} - \rho_i)/(\rho_n - \rho_1)$ represent the relative strengths of the stratification across the interfaces and can vary between zero and one (note that $r_1 + r_2 + \cdots + r_{n-1} = 1$).

The Bernoulli equations (4) in non-dimensional form become

$$J_1 \equiv \frac{1}{2h^2 b^2} \left(\frac{q_1^2}{y_1^2} - \frac{q_2^2}{y_2^2} \right) + r_1 h y_1 - H_1 = 0, \tag{6.1}$$

$$J_2 \equiv \frac{1}{2h^2 b^2} \left(\frac{q_2^2}{y_2^2} - \frac{q_3^2}{y_3^2} \right) + r_2 h (y_1 + y_2) - H_2 = 0, \tag{6.2}$$

$$\vdots$$

$$J_{n-1} \equiv \frac{1}{2h^2 b^2} \left(\frac{q_{n-1}^2}{y_{n-1}^2} - \frac{q_n^2}{y_n^2} \right) + r_{n-1} h (y_1 + y_2 + \cdots + y_{n-1}) - H_{n-1} = 0. \tag{6.n-1}$$

Note that $y_n = 1 - (y_1 + y_2 + \cdots + y_{n-1})$, so we have a system of $(n-1)$ equations in $(n-1)$ variables. In the limit of $n \to \infty$ it can be shown that the system of equations (6) is equivalent to the equations for continuously stratified fluid presented by Benjamin (1981) (equations (4.3) and (4.4) in that paper), except that the upper boundary condition used by Benjamin was a free surface. Note that for given values of the q_i and H_i, the solution for y is dependent only upon the geometric parameters b and h. However, there may be more than one solution for a given set of parameters. To solve the problem we must determine the values of the fluxes q_i, and the Bernoulli constants H_i, such that a solution for y exists along the channel and can be matched to the reservoir conditions.

In the reservoirs where the flow is stagnant the Bernoulli constants H_i are a simple function of the stratification, $H_i = h r_i (y_1 + y_2 + \cdots + y_i)$. In general, however, the stratification is not the same in the two reservoirs and the values of the H_i cannot be the same throughout the channel. The locations at which equations (2) break down and the values of one or more of the H_i change are referred to as hydraulic jumps (Baines 1995).

2.2. *Hydraulic functionals and hydraulic control*

Following the approach of Gill (1977) and Dalziel (1991), we regard the J_i ($i = 1, \ldots, n-1$) as functionals that can be described by

$$\boldsymbol{J}(b, h, q_1, \ldots, q_n, H_1, \ldots, H_{n-1}; y_1, \ldots, y_{n-1}) \equiv \begin{pmatrix} J_1 \\ J_2 \\ \vdots \\ J_{n-1} \end{pmatrix} = \begin{pmatrix} 0 \\ 0 \\ \vdots \\ 0 \end{pmatrix} \equiv \boldsymbol{0}. \tag{7}$$

Solutions to (7) can be traced along the channel by solving

$$\frac{\mathrm{d}\boldsymbol{J}}{\mathrm{d}x} \equiv \begin{pmatrix} \mathrm{d}J_1/\mathrm{d}x \\ \mathrm{d}J_2/\mathrm{d}x \\ \vdots \\ \mathrm{d}J_{n-1}/\mathrm{d}x \end{pmatrix} = \boldsymbol{0}, \tag{8}$$

which can be written as

$$\frac{\mathrm{d}\boldsymbol{J}}{\mathrm{d}x} = \left(\frac{\partial \boldsymbol{J}}{\partial x} \right)_{h,b} + \left(\frac{\partial \boldsymbol{J}}{\mathrm{d}x} \right)_y = \frac{\partial \boldsymbol{J}}{\partial \boldsymbol{y}} \frac{\mathrm{d}\boldsymbol{y}}{\mathrm{d}x} + \frac{\partial \boldsymbol{J}}{\partial \boldsymbol{b}} \frac{\mathrm{d}\boldsymbol{b}}{\mathrm{d}x} = \boldsymbol{0}, \tag{9}$$

or

$$h \boldsymbol{M} \frac{\mathrm{d}\boldsymbol{y}}{\mathrm{d}x} + \boldsymbol{N} \frac{\mathrm{d}\boldsymbol{b}}{\mathrm{d}x} = \boldsymbol{0},$$

where we define $\boldsymbol{M}$ and $\boldsymbol{N}$ as

$$\boldsymbol{M} \equiv \frac{1}{h}\frac{\partial \boldsymbol{J}}{\partial \boldsymbol{y}} \equiv \frac{1}{h}\begin{pmatrix} \dfrac{\partial J_1}{\partial y_1} & \dfrac{\partial J_1}{\partial y_2} & \cdots & \dfrac{\partial J_1}{\partial y_{n-1}} \\ \dfrac{\partial J_2}{\partial y_1} & \dfrac{\partial J_2}{\partial y_2} & \cdots & \dfrac{\partial J_2}{\partial y_{n-1}} \\ \vdots & \vdots & \ddots & \vdots \\ \dfrac{\partial J_{n-1}}{\partial y_1} & \dfrac{\partial J_{n-1}}{\partial y_2} & \cdots & \dfrac{\partial J_{n-1}}{\partial y_{n-1}} \end{pmatrix} \quad \text{and}$$

$$\boldsymbol{N} \equiv \frac{\partial \boldsymbol{J}}{\partial \boldsymbol{b}} \equiv \begin{pmatrix} \dfrac{\partial J_1}{\partial b} & \dfrac{\partial J_1}{\partial h} \\ \dfrac{\partial J_2}{\partial b} & \dfrac{\partial J_2}{\partial h} \\ \vdots & \vdots \\ \dfrac{\partial J_{n-1}}{\partial b} & \dfrac{\partial J_{n-1}}{\partial h} \end{pmatrix}, \qquad (10)$$

and†

$$\frac{\mathrm{d}\boldsymbol{y}}{\mathrm{d}x} \equiv \begin{pmatrix} \dfrac{\mathrm{d}y_1}{\mathrm{d}x} \\ \vdots \\ \dfrac{\mathrm{d}y_{n-1}}{\mathrm{d}x} \end{pmatrix} \quad \text{and} \quad \frac{\mathrm{d}\boldsymbol{b}}{\mathrm{d}x} \equiv \begin{pmatrix} \dfrac{\mathrm{d}b}{\mathrm{d}x} \\ \dfrac{\mathrm{d}h}{\mathrm{d}x} \end{pmatrix}, \quad \text{with} \quad \boldsymbol{y} \equiv \begin{pmatrix} y_1 \\ \vdots \\ y_{n-1} \end{pmatrix}$$

$$\text{and} \quad \boldsymbol{b} \equiv \begin{pmatrix} b \\ h \end{pmatrix}. \quad (11)$$

The functions $\boldsymbol{J}(\cdot\,;\boldsymbol{y})$ map the $(n-1)$-dimensional $\boldsymbol{y}$-space onto the $(n-1)$-dimensional $\boldsymbol{J}$-space. As is necessary for hydraulic-type problems, there are multiple solutions (in $\boldsymbol{y}$-space) to $\boldsymbol{J} = \boldsymbol{0}$ (equation (7)) at a given point along the channel. If the solution remains on the same solution branch as we move along the channel, then a symmetric channel will yield symmetric solutions for the interface heights. To satisfy asymmetric reservoir conditions the solution must pass from one branch to another. For this to happen there must be positions along the channel where there are coincident solutions, and thus where the determinant of the Jacobian is zero, i.e.

$$\det(\boldsymbol{M}) = 0. \qquad (12)$$

Below we show that at least one internal wave mode is stationary there and the flow is said to be 'controlled'.

Where the flow is controlled, the components of equation (9) are not independent. Thus there is a non-zero vector $\boldsymbol{\lambda} = (\lambda_1, \ldots, \lambda_{n-1})$ which satisfies

$$\lambda_1 \frac{\partial J_1}{\partial y_i} + \lambda_2 \frac{\partial J_2}{\partial y_i} + \cdots + \lambda_{n-1}\frac{\partial J_{n-1}}{\partial y_i} = 0, \quad i = 1, \ldots, n-1, \qquad (13)$$

† For cross-sections more complex than the rectangular shape used here, the vector $\boldsymbol{b}$ may be of larger dimension, depending on the number of parameters required to describe the geometry.

and so for a solution to exist at this point,

$$\lambda_1 \frac{\partial J_1}{\partial x} + \lambda_2 \frac{\partial J_2}{\partial x} + \cdots + \lambda_{n-1} \frac{\partial J_{n-1}}{\partial x} = 0. \tag{14}$$

Following the nomenclature used for two-layer flows we refer to equation (14) as the regularity condition.

If there is a constriction in the sense that

$$\frac{\mathrm{d}\boldsymbol{b}}{\mathrm{d}x} = \boldsymbol{0}, \tag{15}$$

then the second term in equation (9) is zero and so either the flow is controlled there or all the interfaces are horizontal ($\mathrm{d}\boldsymbol{y}/\mathrm{d}x = 0$) and the flow is symmetric about the constriction (see Baines 1988). We shall refer to a control at which (15) is satisfied as a geometric control, while all other controls are referred to as virtual controls. In what follows, we shall assume that (15) is satisfied at $x = 0$ and nowhere else.

Note that when (15) is satisfied, (14) is also satisfied. Thus at a geometric control the flow must satisfy (12), but at a virtual control both (12) and (14) must be satisfied. However, although there is an additional equation for a virtual control, there is also an additional unknown: x_v, the location of the control.

2.3. *Froude numbers, wave speeds and information propagation*

Froude numbers for each layer can be defined as

$$F_i^2 = \frac{u_i^2}{g'h_i}, \quad i = 1,\ldots,n, \tag{16a}$$

and in terms of the non-dimensional fluxes and depths these become

$$F_i^2 = \frac{q_i^2}{b^2 h^3 y_i^3}, \quad i = 1,\ldots,n, \tag{16b}$$

The derivatives in the matrix $\boldsymbol{M}$ can be expressed in terms of these Froude numbers:

$$\frac{1}{h}\frac{\partial J_i}{\partial y_j} = \begin{cases} r_i, & j < i \\ r_i - F_i^2, & j = i \\ F_{i+1}^2, & j = i+1 \\ 0, & j > i+1 \end{cases} \quad \text{for} \quad i = 1,\ldots,n-2, \tag{17a}$$

while the final row in the matrix is given by

$$\frac{1}{h}\frac{\partial J_{n-1}}{\partial y_j} = \begin{cases} r_{n-1} - F_n^2, & j < n-1, \\ r_{n-1} - F_n^2 - F_{n-1}^2, & j = n-1. \end{cases} \tag{17b}$$

Conversely, the Froude numbers can be written in terms of the derivatives in various forms, for example

$$\left.\begin{aligned} F_i^2 &= r_i - \frac{1}{h}\frac{\partial J_i}{\partial y_i}, \quad i < n-2, \\ F_{n-1}^2 &= \frac{1}{h}\frac{\partial J_{n-1}}{\partial y_j} - \frac{1}{h}\frac{\partial J_{n-1}}{\partial y_{n-1}} \quad \text{for any} \quad j < n-1, \\ F_n^2 &= r_{n-1} - \frac{1}{h}\frac{\partial J_{n-1}}{\partial y_j} \quad \text{for any} \quad j < n-1. \end{aligned}\right\} \tag{18}$$

We now look for unsteady small perturbations to the steady solutions by assuming that the layer velocities and depths are given by

$$u_i = \hat{u}_i + u'_i \quad \text{and} \quad h_i = \hat{h}_i + h'_i, \quad i = 1, \ldots, n, \tag{19}$$

where $\hat{u}_i$, $\hat{h}_i$ ($i = 1, \ldots, n$) represent the steady solution and the perturbations are of the form $u'_i = u'_i(x - ct)$ and $h'_i = h'_i(x - ct)$, where c is the phase speed of the perturbation. Below we show that there are multiple solutions for c, corresponding to different wave modes. Integrating the linearized versions of equations (2), and taking the differences of pairs of equations gives

$$(\hat{u}_1 - c)u'_1 - (\hat{u}_2 - c)u'_2 + g'_1 h'_1 = 0, \tag{20.1}$$

$$(\hat{u}_2 - c)u'_2 - (\hat{u}_3 - c)u'_3 + g'_2(h'_1 + h'_2) = 0, \tag{20.2}$$

$$\vdots$$

$$(\hat{u}_{n-1} - c)u'_{n-1} - (\hat{u}_n - c)u'_n + g'_{n-1}(h'_1 + h'_2 + \cdots + h'_{n-1}) = 0, \tag{20.n–1}$$

while continuity gives

$$(\hat{u}_i - c)h'_i + \hat{h}_i u'_i = 0, \quad i = 1, \ldots, n. \tag{21}$$

We also have $h'_1 + h'_2 + \cdots + h'_n = 0$. Eliminating the velocity perturbations, we are left with a set of equations for the layer depth perturbations:

$$\left. \begin{aligned} -\frac{(\hat{u}_1 - c)^2}{\hat{h}_1} h'_1 + \frac{(\hat{u}_2 - c)^2}{\hat{h}_2} h'_2 + g'_1 h'_1 &= 0, \\ \vdots \\ -\frac{(\hat{u}_{n-1} - c)^2}{\hat{h}_{n-1}} h'_{n-1} + \frac{(\hat{u}_n - c)^2}{\hat{h}_n} h'_n + g'_{n-1}(h'_1 + \cdots + h'_{n-1}) &= 0, \end{aligned} \right\} \tag{22}$$

which can be written together (using $-h'_n = h'_1 + h'_2 + \cdots + h'_{n-1}$) as

$$\boldsymbol{M}_c \boldsymbol{h}' = \boldsymbol{0}, \tag{23}$$

where

$$\boldsymbol{h}' = \begin{pmatrix} h'_1 \\ \vdots \\ h'_{n-1} \end{pmatrix},$$

and $\boldsymbol{M}_c$ is the same matrix as $\boldsymbol{M}$, but with the F_i replaced by f_i, where

$$f_i^2 = \frac{(\hat{u}_i - c)^2}{g' \hat{h}_i}. \tag{24}$$

Note that when $c = 0$, $f_i = F_i$ and $\boldsymbol{M}_c = \boldsymbol{M}$.

From equation (23), the wave speed, c, must satisfy,

$$\det(\boldsymbol{M}_c) = 0. \tag{25}$$

This is a $2(n - 1)$-polynomial equation for c. At a control, $c = 0$ is clearly one of the solutions of equation (25), since $\det(\boldsymbol{M}) = 0$ there, and thus (at least) one of the

modes is stationary at the control. Equations similar to (23) and (25) were derived by Baines (1988) in the context of multi-layer flow over topography.

3. Solutions for three-layer flow

3.1. *Three-layer theory* ($n = 3$)

For three layers we have $r_1 + r_2 = 1$. The functionals J_1 and J_2 are as given in equations (6.1) and (6.2). We can recover the functional used for two-layer flow (Dalziel 1991) by summing these to give

$$J_{1+2} \equiv \frac{1}{2h^2 b^2} \left(\frac{q_1^2}{y_1^2} - \frac{q_3^2}{y_3^2} \right) + hy_1 + r_2 hy_2 - H_{1+2} = 0, \tag{26}$$

and then setting the middle layer depth to zero ($y_2 = 0$). Returning to three-layer flow, the matrix $\boldsymbol{M}$ is given by†

$$\boldsymbol{M} = \begin{pmatrix} r_1 - F_1^2 & F_2^2 \\ r_2 - F_3^2 & r_2 - F_2^2 - F_3^2 \end{pmatrix}, \tag{27}$$

and the regularity condition becomes,

$$\left(\frac{\partial J_1}{\partial y_i} \right) \left(\frac{\partial J_2}{\partial x} \right)_y = \left(\frac{\partial J_1}{\partial x} \right)_y \left(\frac{\partial J_2}{\partial y_i} \right), \quad i = 1, 2. \tag{28}$$

The equation for the wave speed, $\det(\boldsymbol{M}_c) = 0$, is a quartic in c. If the four solutions are real, two will correspond to the first mode with perturbations to the interfaces having the same sign (and thus h_1', and $h_1' + h_2'$ having the same sign) so that

$$r_1 \leqslant f_1^2 + f_2^2 \quad \text{and} \quad r_2 \leqslant f_3^2 + f_2^2, \tag{29a}$$

while for the second mode h_1' and $h_1' + h_2'$ have opposite signs and so

$$r_1 \geqslant f_1^2 + f_2^2 \quad \text{and} \quad r_2 \geqslant f_3^2 + f_2^2. \tag{29b}$$

We now consider three-layer exchange flow through a pure contraction (with no change in channel depth) with the interface depths in the reservoirs specified.

3.2. *Finding solutions*

In this section the procedure used to determine solutions for given reservoir conditions is outlined. The numerical methods used to calculate the solutions presented are described in Appendix A.

In general, the stratifications in the two reservoirs will be different. In this case the flow in the channel will be connected to the reservoirs via one or more hydraulic jumps. There are two stages in solving for the flow. First, the Bernoulli potentials and the appropriate branches for the flow in the channel must be determined. Second, the functional equation (7) must be solved to find the values of the fluxes and the detailed structure of the flow in the channel. However, as we shall see in the following examples, a knowledge of the solutions of the functional equations is needed for the first stage as well as the second.

When invoking hydraulic jumps we require that the flow is supercritical with respect

---

† The equations here appear different from those in Smeed (2000). This is because we choose here to use y_1 and y_2 as the independent variables (to be consistent with the multi-layer formulation) whereas Smeed (2000) uses y_1 and y_3.
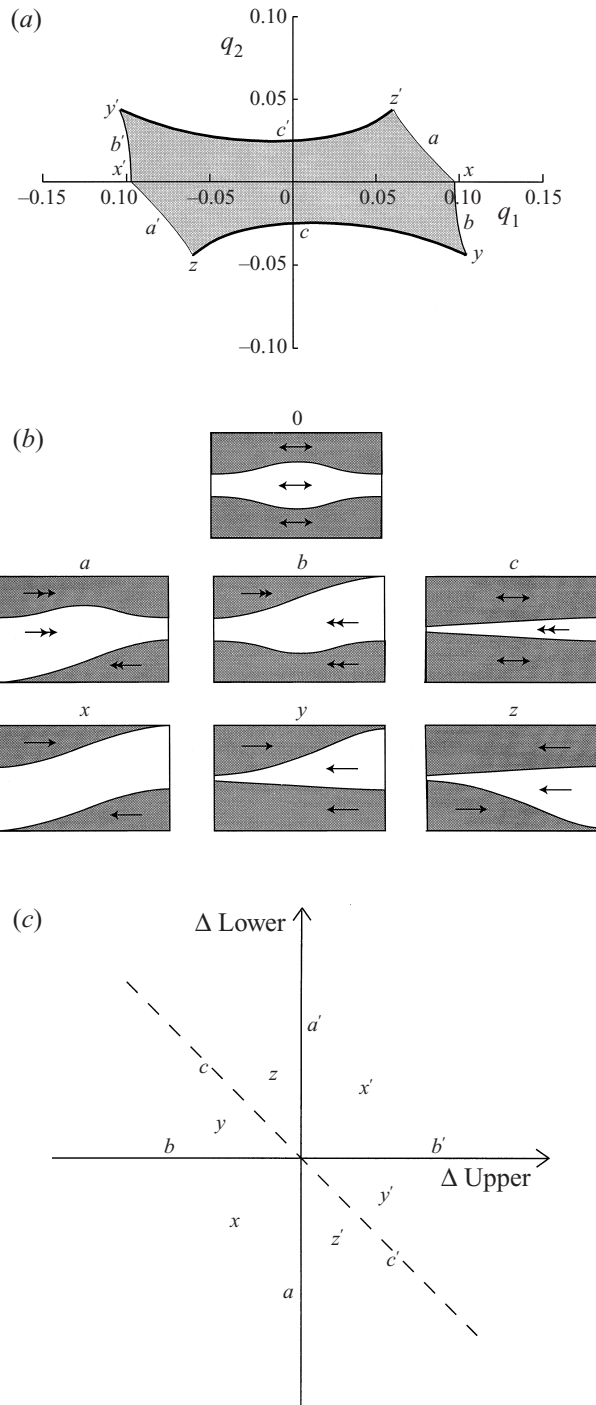
FIGURE 3. (*a*) Solutions in the (q_1, q_2)-plane. The parameter $r_1 = 0.5$ and the Bernoulli constants are those for a static reservoir in which $y_1 = 0.4$ and $y_2 = 0.2$ (i.e. $H_1 = 0.2$ and $H_2 = 0.3$). The six curves a, a', b, b', c, c' indicate solutions for which there is one control. For each of these the flow is subcritical to one side of $x = 0$ and one mode is supercritical on the other. The points x, x', y, y', z, z' indicate solutions with two controls for which the flow is supercritical in both reservoirs. Between the controls the flow is subcritical (unless the controls are coincident as in y, y'). (*b*) Sketches indicating

to at least one mode on one side of the jump and subcritical on the other side of the jump, and that there be no net gain in energy at the jump.

When the stratification is the same in the two reservoirs and all the layer depths are $O(1)$ then the Bernoulli constants H_1 and H_2 are determined by the reservoir conditions and take the same values for all x. In this case solutions can be found for a surface on the (q_1, q_2)-plane (see, for example, figure 3). On the boundary of the domain in the (q_1, q_2)-plane for which such solutions are possible the flow becomes critical at $x = 0$. Note that in the lock exchange configuration used in the experiments the actual flow realized (starting with the same interface depths in both reservoirs) would be one of no flow, i.e. $q_1 = q_2 = 0$.

If one interface has the same in height in both reservoirs but the other has different values then there must be a hydraulic jump at which the Bernoulli constant can change. Hydraulic jumps are a transition from supercritical to subcritical flow. However, the flow in both reservoirs is subcritical and so the supercritical flow can only occur in a bounded interval. There must therefore be a second transition and this occurs at a control. One control reduces the number of degrees of freedom by one and so solutions can only be found on a line in the (q_1, q_2)-plane. In this case both modes are subcritical upstream of the control and one mode is supercritical downstream of the control.

There are three possible branches on which one mode is supercritical, and the correct branch must be determined. On each branch one of the layer depths tends to zero as the width of the channel tends to infinity. For the example in figure 3, $a, b,$ and c illustrate the three possible solutions of this type. Reservoir conditions for which each of these can occur are indicated in figure 3(c). Further details are given in Appendix B.

When both interfaces have different heights in the two reservoirs then there must be at least two controls. This further reduces the degrees of freedom so that flows with two controls can only be found at points in the (q_1, q_2)-plane. There are two sorts of flow with two controls. In the first there are two regions in the channel in which one mode only is supercritical, separated by a region in which either the flow is subcritical or both modes are supercritical. In the second there is region in which both modes are supercritical and a region in which both modes are subcritical; these regions are separated by a region in which one mode only is supercritical.

For small changes in the reservoir conditions in the example of figure 3, flows of the first type will occur. These are illustrated in types $x, y,$ and z. Further details are given in Appendix B. The reservoir conditions for which these flows could occur are illustrated in figure 3(c). Note however, that for large changes to the reservoir conditions different flow types may occur. These will be either of the second type with two controls described above or of a type in which there are three controls. These flow types are illustrated in figure 14 of Appendix B; however, a complete description of the reservoir conditions for which they occur is beyond the scope of this paper.

Flows with three controls are analogous to the maximal two-layer flows. Only one

the form of the solutions for the flow types a, b, c, x, y and z. Double arrowheads indicate that the magnitude, and in some cases, direction of flow is variable. Note that the solutions a', b', c', y' and z' are obtained by reflection about $x = 0$. (c) Illustration of how perturbing the basic state (in which both reservoirs have the same stratification) gives rise to the different flow types in the channel. (There is no scale on this plot, since the results are only valid for small perturbations about the basic state.)
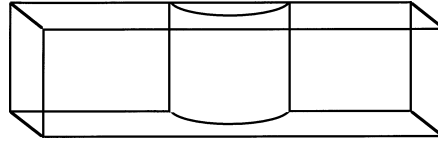
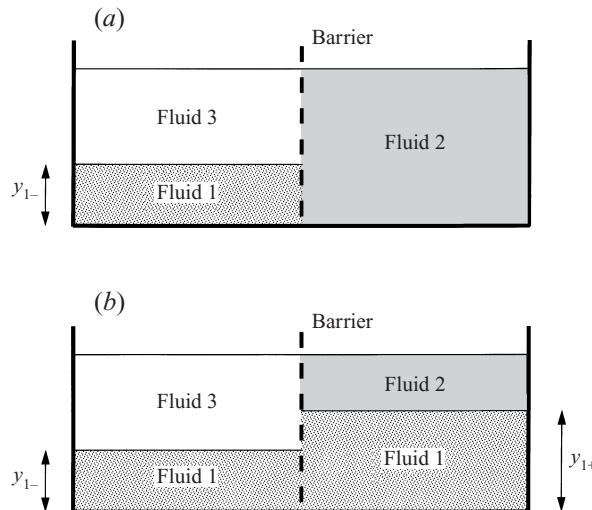FIGURE 4. Sketch of the apparatus used for the laboratory experiments.

FIGURE 5. The stratification used in the laboratory experiments (*a*) for case A, (*b*) for case B. Note that the stratification is inverted compared with the Red Sea (figure 1) for experimental convenience.

of the Bernoulli constants is set by the reservoir conditions, the other is determined by the solution for the flow in the channel.

4. Experiments

We will concentrate on flows analogous to the Red Sea flow, with the upper layer present in both reservoirs, while the middle layer is not present (initially) in one reservoir and the densest layer is not present in the other (i.e. $y_{2-} = 0$ and $y_{3+} = 0$).

4.1. *Apparatus*

The experiments were conducted in a rectangular Perspex tank 13 cm wide, 116 cm long and 29 cm high. The tank was divided into two reservoirs by a smoothly curved contraction formed using a D-shaped insert (figure 4). At the centre of the contraction the channel width was reduced to 5 cm. A thin barrier was placed at this point before the tank was filled, and the experiment was started by removing the barrier. The fluids used were fresh water and salt solutions, with densities ranging from 1.00 to 1.15 g cm^{-3}.

For each experiment the tank was first filled to the appropriate depth with the densest fluid to be used. Lighter fluid was then added by introducing the fluid slowly through a cut-out sponge floating on the surface. In the simplest case (case A; figure 5*a*), the densest fluid was present only on one side of the barrier, with the lightest fluid above it and only fluid of intermediate density on the other side of the barrier.

Typically, however, the densest fluid (fluid 1) was present on both sides of the barrier, though with different depths either side of the barrier (case B). The lightest fluid (fluid 3) was placed above the dense fluid on one side of the barrier while fluid of intermediate density (fluid 2) was placed above the dense fluid on the other side of the barrier (figure 5b). This arrangement is effectively an inversion of the Bab al Mandab conditions, where it is the lightest, surface, layer that is present on both sides of the constriction. For this reason we use y_1 to denote the thickness of the densest layer in the experiments.

Two visualization techniques were used. In the main technique there was general lighting with a white background behind the tank and the various parts of the fluid were marked with dyes. For some experiments a sheet of light, parallel with the long side of the tank, was used. The light sheet was generated by a conventional slide projector, with the light reflected up through the tank by a thin mirror. In this case the fluids were marked with fluorescent dye and particles. The particles were pliolite, of density between 1.02 and 1.03 g cm^{-3} and diameter approximately 0.5 mm. The particles allowed direct measurement of the fluid velocities.

The experiments were recorded using a video system and analysed with DigImage software (Dalziel 1992b). The digitized images consisted of arrays of 512×512 pixels, with intensities recorded as integers between 0 and 255. The positional accuracy depends on the field of view: for the experiments with general lighting, positions were measured to ± 0.2 mm, while a smaller field of view gave an error of ± 0.1 mm for the light sheet experiments. For the experiments with general lighting, fluxes were estimated from the flow beyond the contraction by measuring the speed and thickness of the currents generated there. For the light sheet experiments the fluxes were estimated from velocities and thicknesses measured at the centre of the contraction. In addition to basic measurement errors, there is some uncertainty in defining an interface position between miscible layers and (for the light sheet experiments) in finding the velocity at the contraction where the flow is accelerating. The overall error in any flux measurement we estimate to be 10% of the largest layer flux.

For most of the experiments the density difference between fluid 1 and fluid 2 was equal to that between fluid 2 and fluid 3, i.e. $r_1 = 0.5$. A set of experiments was also conducted with $r_1 = 0.67$, i.e. with the density difference between fluid 1 and fluid 2 twice that between fluid 2 and fluid 3. A selection of interface heights covering the possible cases was used, with particular concentration on the cases where the interface between fluid 1 and fluid 3 is at half the total depth ($y_{1-} = 0.5$). The two-fluid exchange flows are all equivalent: $(y_{1-}, y_{1+}) = (0, 0), (1, 0)$ or $(0, 1)$ and r_1 set to any value are all the same, subject to suitable rescaling.

4.2. *General features*

The removal of the barrier generates a small amount of motion and mixing, but the flow quickly accelerates to a quasi-steady exchange flow. The initial acceleration time scale $(H/g')^{1/2}$ is 1–2 s, while the time taken for the flow to be established throughout the contraction is $L/(g'H)^{1/2}$, where L is the length of the contraction, and is also of the order of 1–2 s. In general the fluid of intermediate density flows as an intrusion in one direction, while the other fluids flow in the opposite direction above and below; thus there are usually two interfaces at the constriction. For some parameters, the densest fluid flows in the same direction as the intermediate fluid, and there are also cases where one layer is stationary. Examples of the flows are shown in figure 6.

The exchange flows are not completely steady because the flow alters the conditions in the reservoirs, which in turn may alter the flow at the constriction. However, where
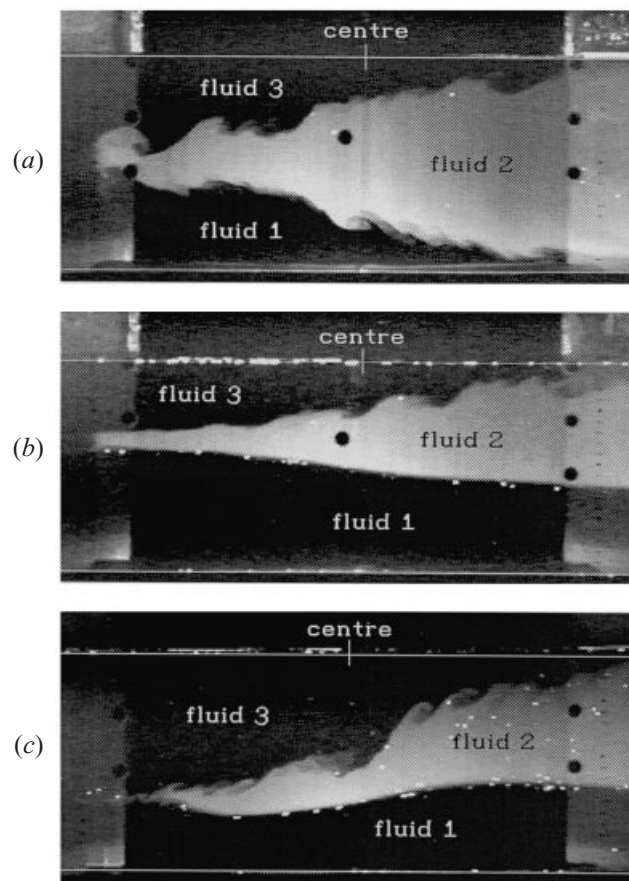
FIGURE 6. Examples of flows through the constriction with fluid 2 dyed with fluorescein and lit by a sheet of light. (*a*) Initially no fluid 1 to the right of the barrier (an example of case A flow, $y_{1-} = 0.5$, $y_{1+} = 0$); interfacial waves formed on both interfaces. (*b*) Fluid 1 present on both sides of the barrier (an example of case B flow. $y_{1-} = 0.5$, $y_{1+} - 0.5$); for these parameters interfacial waves form on the upper interface only, (*c*) Another case B flow ($y_{1-} = 0.25$, $y_{1+} = 0.5$); interfacial waves are present on the upper interface and there is a small hydraulic jump on the lower interface to the left of the contraction.

the flow is supercritical between the constriction and the reservoir (typically with a hydraulic jump to match the channel and reservoir flows), then changing reservoir conditions will not alter the exchange flow. Even if the flow is subcritical we can still make useful estimates of interface heights and fluxes at the constriction, provided the reservoir conditions are not changing too rapidly.

The interfaces were often seen to be unstable to interfacial waves, with these waves generally propagating away from the constriction. For two-layer flows, critical conditions are necessary (but not sufficient) for instability (Dalziel 1991). Where waves are visible on both interfaces we take this as indicating a fully controlled flow with supercritical conditions either side of the control. If at least one interface is smooth then we take this to indicate that the flow is possibly not fully controlled. These waves are described and discussed further in §6. If the flow is not fully controlled, then it may respond to the changing reservoir conditions and we do not have a properly steady flow at the constriction.
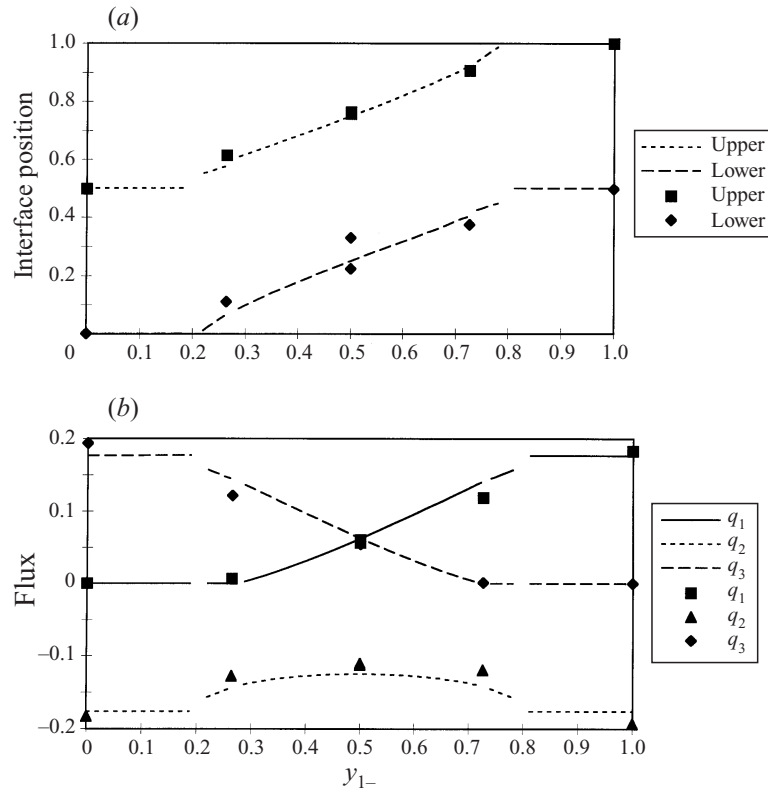
FIGURE 7. Results from the theory (lines) and laboratory experiments (symbols) for flows with only fluid 2 to the right of the barrier (case A: $y_{1+} = 0$) showing the variation of (*a*) interface heights and (*b*) fluxes with the position of the interface to the left of the barrier, y_{1-}. The density differences across the two interfaces are equal, i.e. $r_1 = 0.5$.

5. Results

In this section we illustrate the three-layer exchange flows resulting from several sets of reservoir conditions (defined in figure 5) and describe the dependence of the flow upon the parameters describing the stratification. As mentioned above, all the flows have $y_{2-} = y_{3+} = 0$, i.e. fluid 2 not present to the left of the constriction, fluid 3 not present to the right.

5.1. *Case A*

In these experiments the fluid in the right-hand reservoir was of uniform density, ρ_2, i.e. $y_{1+} = 0$. In the left-hand reservoir there was a two-layer stratification with fluids of density ρ_1 and ρ_3. Thus only two (independent) parameters are required to describe the initial conditions: the stratification parameter, r_1, and the height of the interface in the left-hand reservoir, y_{1-}. The results presented here are for the case $r_1 \approx 0.5$.

If the flux in a given layer is non-zero and that layer has vanishing thickness in a reservoir, then the Froude number for that layer $\rightarrow \infty$ and it can be shown that the flow must be supercritical with respect to at least one mode (Smeed 2000). If one layer (with non-zero flux) is vanishingly thin the flow is supercritical with respect to only one mode, while if two layers are vanishingly thin the flow is supercritical with respect to both internal modes. In reality, the flow in the reservoirs will be subcritical,

the layers will have small but finite thickness, and hydraulic jumps will be required to connect the reservoirs to the channel flow.

For our case A, the appropriate solution approaching the left-hand reservoir is the branch of equations (9) with one-mode supercritical and with the depth of layer 2 tending to zero ($y_{2-} \to 0$). The appropriate solution approaching the right-hand reservoir is one for which $y_{1+} \to 0$ and $y_{3+} \to 0$; in this case both the modes are supercritical. The conditions in the left-hand reservoir prescribe $H_1 + H_2$, but the remaining three parameters, q_1, q_2, and $H_1 - H_2$, are determined by the conditions at the three controls. Note that two of the controls coincide at $x = 0$. This is in contrast to the case of a sill (Smeed 2000) for which the controls are not coincident.

According to the theoretical results (for $r_{1-} = 0.5$), there is a non-zero flux in all layers for $0.27 < y_{1-} < 0.73$. For $y_{1-} \leqslant 0.27$ solutions of the above form cannot be found. Instead layer 1 is arrested, while layer 3 is arrested for $y_{1-} \geqslant 0.73$. However, the arrested fluid is still present in the centre of the channel as an arrested wedge for $0.20 < y_{1-} < 0.27$ and $0.73 < y_{1-} < 0.80$, similar to arrested wedges in forced two-layer flows. As $y_{1-} \to 0.27^+$ (i.e. from above), the virtual control $x_v \to \infty$. For $y_{1-} = 0.27$, the depth of layer 1 vanishes as $x \to \infty$; while for $y_{1-} < 0.27$ the depth of layer 1 vanishes at a point x_w, with $x_w \to \infty$ as $y_{1-} \to 0.27^-$, $x_w = 0$ for $y_{1-} = 0.20$ and $x_w \to -\infty$ as $y_{1-} \to 0^+$.

Experimental and theoretical results (interface heights at the constriction and layer fluxes) for $y_{1+} = 0$, with $0 \leqslant y_{1-} \leqslant 1$, are shown in figure 7. The interfaces at the contraction rise in response to a higher interface in the left-hand reservoir. The flux in the intermediate intruding layer is fairly constant, while the flux in each of the other two layers increases with increasing thickness of that layer in the reservoir. There is good agreement between the experiments and the theory.

5.2. *Case B*

In these experiments the left-hand reservoir again has a two-layer stratification (with fluids of density ρ_1 and ρ_3), but the right-hand reservoir now also has a two-layer stratification (but with fluids of density ρ_1 and ρ_2), i.e. $y_{1+} \neq 0$. In this case three parameters are required to describe the initial conditions: the stratification r_1, and the heights of the interfaces in the reservoirs, y_{1-} and y_{1+}. Most of the experiments were with flows where the density differences $\rho_1 - \rho_2$ and $\rho_2 - \rho_3$ were equal, $r_1 \approx 0.5$, so that the density of fluid 2 is the mean of fluids 1 and 3.

5.2.1. $y_{1-} = 0.5$ *and* $0 \leqslant y_{1+} \leqslant 1$

The experimental and theoretical results for the case $y_{1-} = 0.5$ with $0 \leqslant y_{1+} \leqslant 1$ are shown in figure 8. For $y_{1+} = 1$ there is no fluid 2 and the flow is the maximal two-layer exchange between layers 1 and 3.

For y_{1+} a little less than 1 the fluxes in the layers are the same as for $y_{1+} = 1$, but there is a stagnant wedge of fluid 2 to the right of the contraction. As y_{1+} is decreased the nose of the wedge moves towards the constriction. According to the theory the nose of the wedge is at $x = 0$ for $y_{1+} = 0.75$. Decreasing y_{1+} further reduces the flux in layers 1 and 3, and increases the depth of layer 2 at the contraction but, according to the theory, there is no flux in layer 2 until $y_{1+} = 0.5$. The values of y_{1+} at which these transitions occur in the experiments agree well with the theory, but other parameters, for example the flux in layers 1 and 3, differ significantly from the theory.

In fact the experimental results for $y_{1+} = 0.5$ are much more closely matched by theoretical results with $y_{1-} = 0.6$ than by the theoretical results with $y_{1-} = 0.5$.
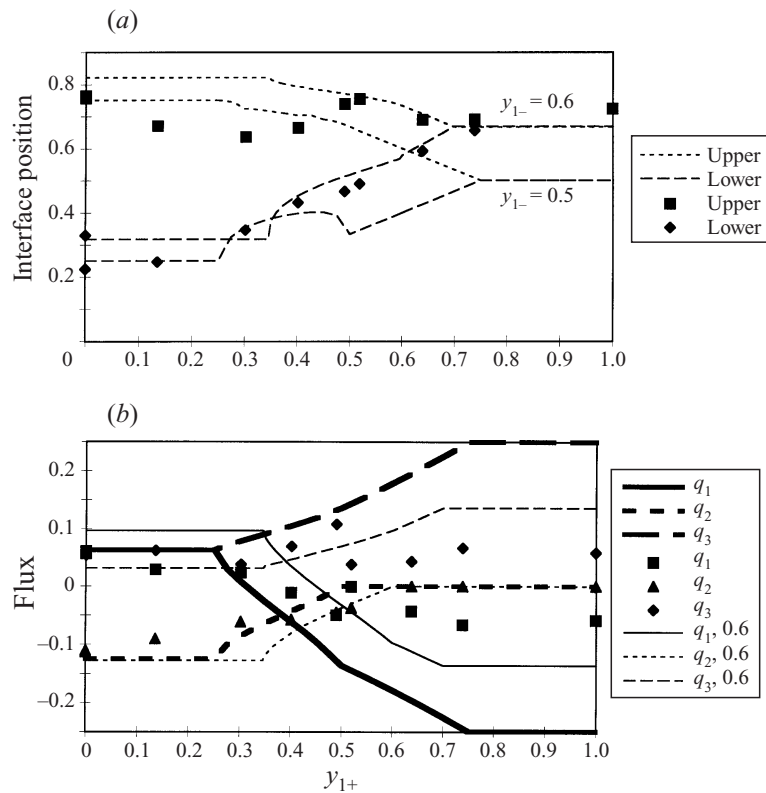
FIGURE 8. Results from the theory (lines) and laboratory experiments (symbols) for flows with the interface to the left of the barrier at half the total depth ($y_{1-} = 0.5$), showing the variation of (*a*) interface heights and (*b*) fluxes with the position of the interface to the right of the barrier, y_{1+}. The density differences across the two interfaces are equal, i.e. $r_1 = 0.5$. Also shown are theoretical results for $y_{1-} = 0.6$.

As soon as the experiment is initiated fluid flows from one reservoir to the other, thus changing the reservoir conditions (increasing y_{1-} beyond 0.5). Thus the finite nature of the experimental reservoirs and the absence of fully controlled conditions at the contraction are important in determining the flow observed during most of the experiment. Where the theoretical flow changes sharply for a small change in reservoir conditions (in this case as y_{1-} increases beyond 0.5), care must be taken in interpreting the theoretical results. It is likely that better agreement would be obtained if the volumes of the reservoirs were greater. Also, when the experiment is started bores may propagate away from the contraction, modifying the effective reservoir conditions (Lane-Serff & Woodward 2000). However, when the width of the reservoir is much greater than the contraction we expect this effect to be small. The finite volume of the reservoirs is likely to be the most significant factor in the experiments reported here.

Decreasing y_{1+} below 0.5, there is a non-zero flux in layer 2. In the left-hand reservoir the appropriate solution branch of equations (9) is the one with $y_{2-} \to 0$, while in the right-hand reservoir $y_{3+} \to 0$; this is same type of solution as y in figure 3, and there is a bounded region of subcritical flow between the two controls.

According to the theory the flux in layer 2 is a maximum for $y_{1+} = 0.25$. For y_{1+} less than this value a third control is introduced into the flow and one of
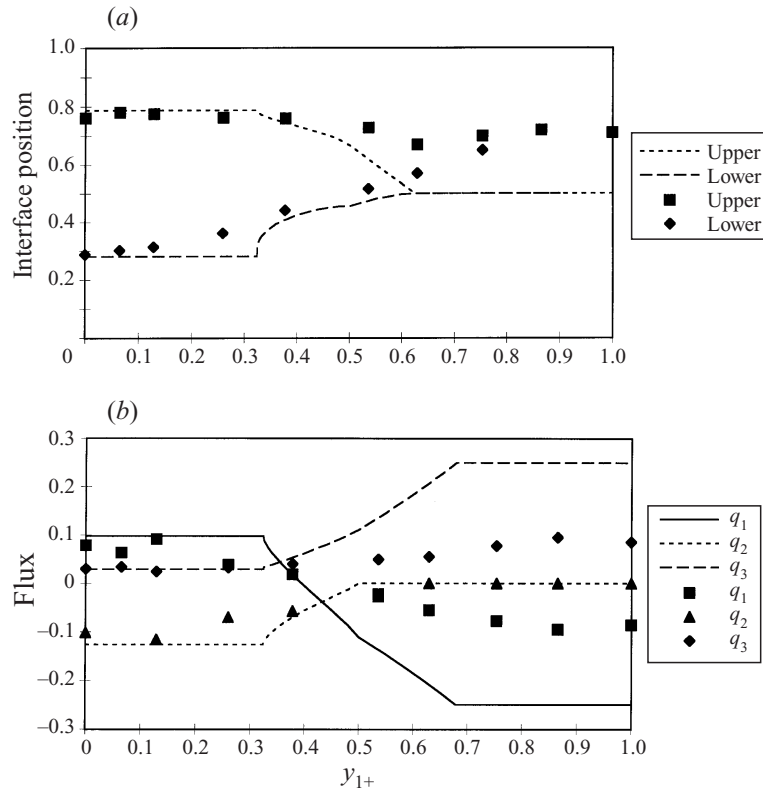
FIGURE 9. Results from the theory (lines) and laboratory experiments (symbols) for flows with the density difference between fluid 1 and fluid 2 twice that between fluid 2 and fluid 3, i.e. $r = 0.67$, for $y_{1-} = 0.5$, showing the variation of (a) interface heights and (b) fluxes with $y_{1+} \leqslant 1$. Compare these results with the equivalent results for $r_1 = 0.5$, figure 8.

the Bernoulli constants is determined by the solution to the hydraulic functional. A hydraulic control is necessary to match the solution to the conditions in the right-hand reservoir. Figure 8 indicates that for $y_{1+} < 0.25$ the agreement is much better than for large values of y_{1+} (when both Bernoulli constants are set by the reservoirs and the flow is thus much more sensitive to the finite size of the reservoirs).

A few experiments were conducted for $y_{1-} = 0.5$ with the density difference between fluid 1 and fluid 2 twice that between fluid 2 and fluid 3 (and thus $r_1 = 0.67$). The results are shown in figure 9. The results are very similar to the corresponding experiments with $r_1 = 0.5$ (figure 8), again highlighting the care that must be taken when close to transition points in the parameter space.

5.2.2. $y_{1+} = 0.5$ and $0 \leqslant y_{1-} \leqslant 1$

Results for $y_{1+} = 0.5$, with $0 \leqslant y_{1-} \leqslant 1$ are shown in figure 10. According to the theory, for $y_{1-} > 0.75$ there is a two-layer exchange between fluids 1 and 2, and a stagnant wedge of layer 3, the apex of which moves towards the constriction as $y_{1-} \rightarrow 0.75$. On decreasing y_{1-} further there is a non-zero flux in layer 3 and a, rapid decrease in the fluxes of fluids 2 and 3. For $0.5 < y_{1-} < 0.75$ there are two controls
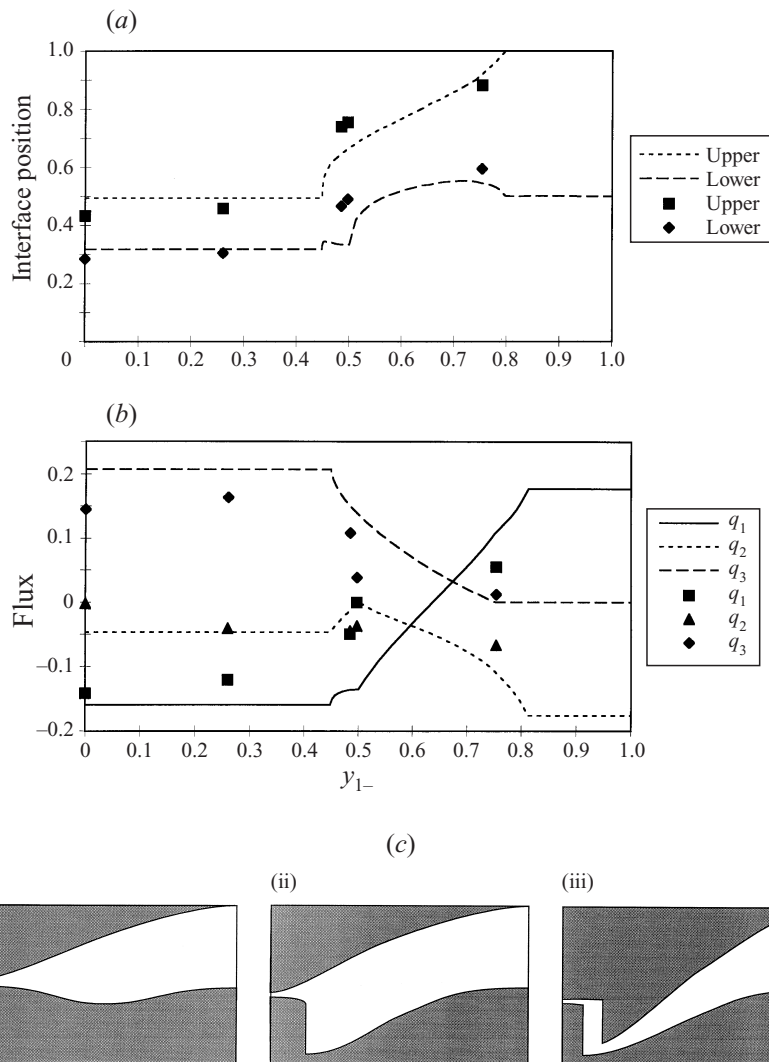
FIGURE 10. Results from the theory (lines) and laboratory experiments (symbols) for flows with the interface to the right of the barrier at half the total depth ($y_{1+} = 0.5$), showing the variation of (*a*) interface heights and (*b*) fluxes with the position of the interface to the left of the barrier, y_{1-}. (*c*) Sketches of the flow types for $y_{1+} = 0.5$ with (i) $y_{1-} \geqslant 0.5$, (ii) $0.5 > y_{1-} \geqslant 0.45$ and (iii) $y_{1-} < 0.45$. The density differences across the two interfaces are equal, i.e. $r_1 = 0.5$.

bounding a subcritical regions between regions in which one mode is supercritical. This is the same as the flow type *y* in figure 3.

For y_{1-} less than 0.5 the flow changes qualitatively to one in which there is a hydraulic jump in the left-hand reservoir. This transition is illustrated schematically in figure 10(*c*). According to the theory there is a second transition at $y_{1-} = 0.45$. For smaller values of y_{1-}, there are three controls and both modes are supercritical before the hydraulic jumps. The case $y_{1+} = 0.5$ and $y_{1-} = 0.25$ is shown in figure 6(*c*). There does indeed seem to be one, or possibly two, hydraulic jumps in the left-hand reservoir. The first, close to the constriction, affects the upper interface principally and the second has a greater effect on the lower

interface. These jumps can be distinguished from the interfacial waves in the experiments because the jumps are stationary whereas the waves are swept away from the contraction.

5.2.3. $0 < y_{1+} < 1$ *and* $0 < y_{1-} < 1$

The interface heights and fluxes for all of the laboratory experiments with $r_1 = 0.5$ are summarized in contour plots in figure 11. A few observations can be made from these plots.

The depth of layer 1 is dependent principally on the average depths of that layer in the two reservoirs (figure 11*a*), and the depth of layer 3 at the contraction is dependent principally on the depth of that layer in the left-hand reservoir (figure 11*b*). The dependences of the fluxes are more complex. However, the flux in layer 1 depends most strongly on the change in depth of that layer between the two reservoirs (figure 11*c*), and the flux in layer 2 depends most strongly upon the depth of that layer in the right-hand reservoir (figure 11*d*). The flux in layer 3 depends mostly upon the depth of that layer in the left-hand reservoir (figure 11*e*).

These trends are broadly in agreement with the theoretical results (as illustrated in figures 8, 9 and 10). The theory does in general indicate greater nonlinearity in the dependence upon the reservoir conditions than is observed.

6. Discussion

6.1. *Instability and waves*

The interfacial waves observed in the laboratory experiments give some information about the character of the flow. Three main types of behaviour were observed (and are summarized on figure 12): (i) waves formed on both interfaces, with the waves propagating and growing away from the constriction in both directions, labelled 'divergent/divergent'; (ii) waves formed only on the interface between fluids 2 and 3 (propagating and growing away from the constriction in both directions) with the other interface smooth, labelled 'divergent/smooth'; (iii) waves formed on the interface between fluids 2 and 3, propagating and growing only to the right, with the other interface smooth or absent at the constriction, labelled 'right/various'.

The three wave regimes observed in the laboratory experiments correspond to three types of theoretical flow, which can be illustrated with three examples: $(y_{1-}, y_{1+}) = (0.5, 0)$, $(0.5, 0.35)$ and $(0.5, 0.65)$. Once the theoretical fluxes and interface heights have been found along the channel, we can solve equation (25) to find the wave speeds at various positions along the channel and use equation (29) to identify the wave modes (see figure 13).

For the first case ($y_{1+} = 0$), the theory implies that the flow is supercritical with respect to mode 2 waves everywhere except at $x = 0$, where it is critical. For mode 1, the flow is subcritical for $x < 0$, and indeed for $x < x_v$, where this mode is critical. To the right of x_v, the flow is supercritical with respect to mode 1. All the wave speeds for this case are real for all x. For the laboratory experiments with these parameters the observed interfacial waves are in the 'divergent/divergent' regime, growing and propagating away from the constriction.

As y_{1+} increases, the flow at the constriction remains the same, with the lower interface undergoing a hydraulic jump to match onto the reservoir condition until, at $y_{1+} = 0.25$, the virtual control is flooded so that for the second case ($y_{1+} = 0.35$) the theory implies that the flow is subcritical with respect to mode 1 everywhere. There is now a virtual control with $x_v < 0$, and to the left of this the flow is supercritical
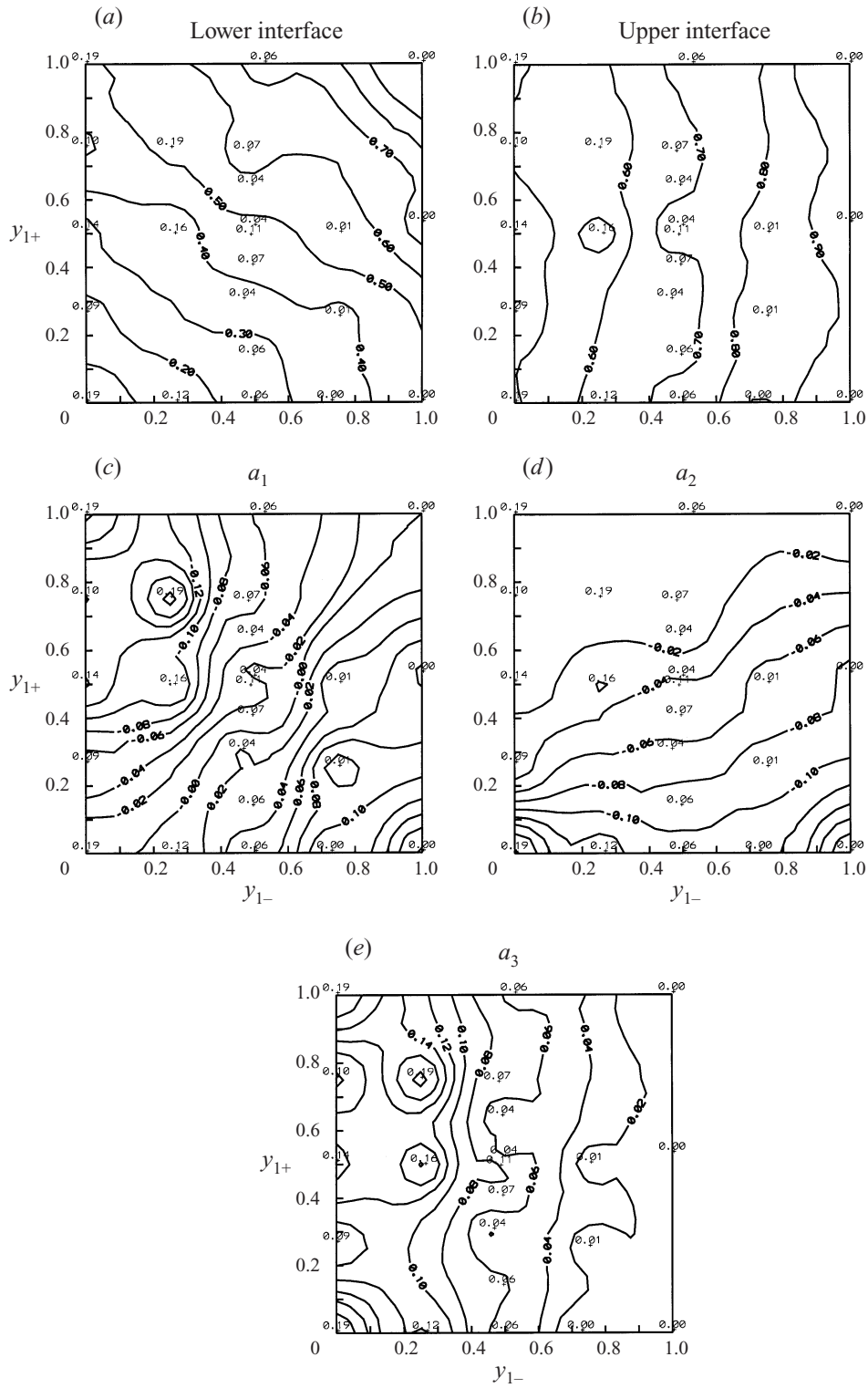
FIGURE 11. Contour plots of results from the laboratory experiments showing (a, b) interface heights and (c, d, e) fluxes as functions of the interface heights to each side of the barrier, y_{1-} and y_{1+} for $r_1 = 0.5$.
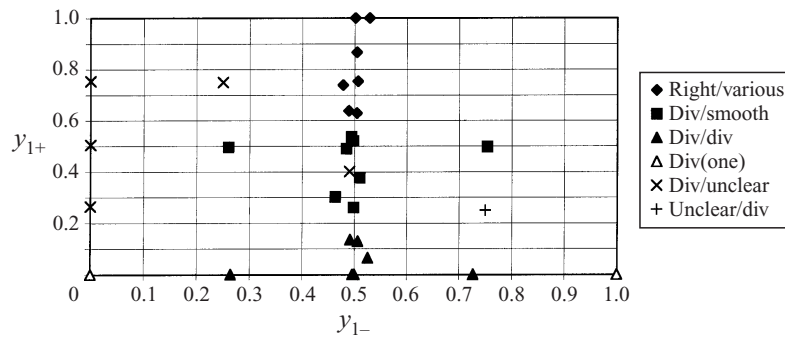
FIGURE 12. Different interfacial wave regimes observed in the laboratory experiments in the (y_{1-}, y_{1+})-parameter space. $r_1 = 0.5$.
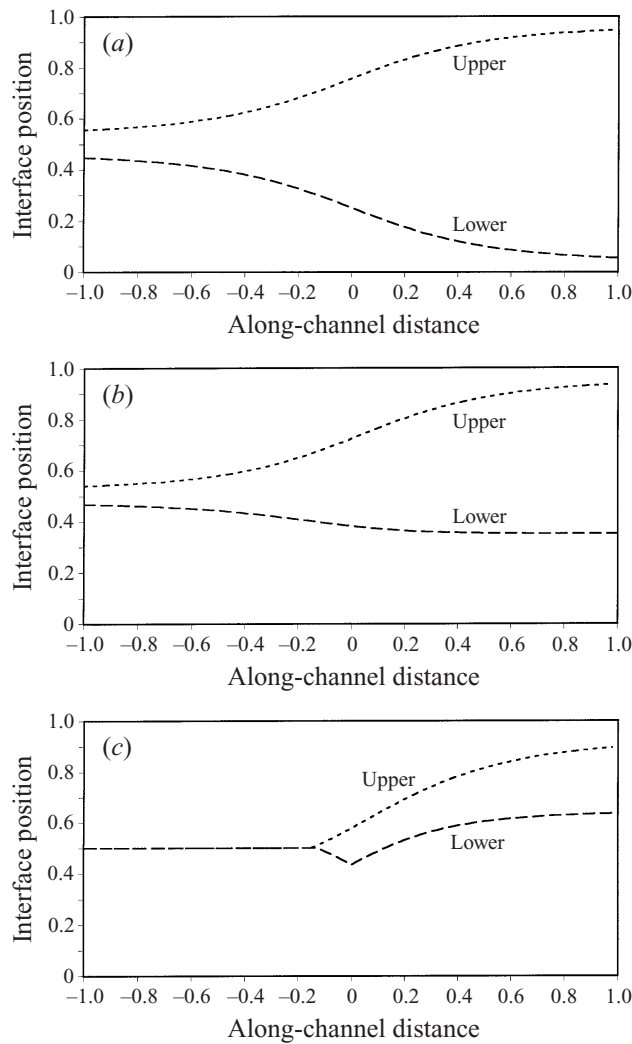

FIGURE 13. Theoretical calculations of the interface positions along the channel for the cases (a) $(y_{1-}, y_{1+}) = (0.5, 0)$, (b) $(0.5, 0.35)$ and (c) $(0.5, 0.65)$. These are similar regimes to the experimental flows in figure 6.

with respect to mode 2. At the virtual control the flow is critical (with respect to mode 2), and then subcritical between the virtual control and $x = 0$. For $x > 0$, the flow is supercritical with respect to mode 2 and the wave speed is complex. The corresponding laboratory experiments are in the 'divergent/smooth' regime with waves on only one of the interfaces.

As y_{1+} increases further, the virtual control moves to the left away from the constriction and layer 2 becomes blocked ($q_2 = 0$). For the third case ($y_{1+} = 0.65$), the flow is subcritical everywhere with respect to mode 1, while it is subcritical with respect to mode 2 to the left of the constriction, critical at $x = 0$ and supercritical (with complex wave speed) for $x > 0$. In this case the laboratory experiments are in the 'right/various' regime, with waves forming on one interface and propagating in one direction only.

Thus, while the different types of observed wave behaviours correspond to different theoretical regimes, the relationship is not straightforward. The observed instabilities are of finite wavelength and amplitude, so not directly related to the theory given here (which is for linear perturbations of long wavelength). Theoretical treatments of stratified shear flow instabilities generally predict fastest growth at short wavelengths. A stability theory including short-wavelength and finite-amplitude perturbations may give more accurate predictions.

6.2. *Oceanographic implications*

The laboratory and theoretical results illustrate how the flow through the constriction responds to changes in the density structure in the two reservoirs. In particular, we can identify the conditions necessary for flow in one or other of the layers to be arrested or reversed. In the context of the Red Sea, the changes in the observed flow in response to the monsoon winds can be interpreted in terms of the changes in the interface depths. The main change in the stratification on each side of Bab al Mandab between the winter and summer monsoon is that upwelling in the Gulf of Aden during the summer monsoon results in a much shallower surface layer there (see figure 1). In terms of our non-dimensional notation, the interface on the Red Sea side of the strait remains approximately constant ($y_{1-} \approx 0.5$), while y_{1+} changes from a large value in the winter to a smaller value in the summer. Referring to figure 8, we can see that these changes in the interface positions account for changes in the flow direction of fluid 1 (the surface layer in Bab al Mandab) and the arresting of fluid 2 (the Gulf of Aden intermediate water), as well as changing the strength of the outflow of Red Sea Overflow Water. In addition to the change in interface level, there is also a seasonal change in the density of the surface water and thus in the relative strengths of the interfaces, with r_1 varying from approximately 0.5 (in the winter) to approximately 0.67 (in the summer). Further details are given in Smeed (1997, 2000).

More generally, the accurate representation of flow through straits in ocean circulation models is very challenging, because the resolution is usually inadequate. The hydraulic approach we give here provides a possible method for parameterizing these flows. This approach is particularly suited to isopycnic models, in which the stratification is already expressed in terms of the thickness of discrete layers of fixed density. The laboratory experiments draw attention to the care that must be taken in using such a theoretical model. For some flows small changes in reservoir conditions and effects not included in the model (e.g. viscosity, rotation) may result in flows with substantially different fluxes than initially predicted.

7. Summary and conclusions

We have extended hydraulic control theory to flows with multiple layers, which allows the calculation of flows through a constriction driven by the stratification on each side of the constriction. This powerful technique is illustrated with detailed calculations for some three-layer pure exchange flows (i.e. zero net flux), which give reasonable agreement with a corresponding set of laboratory experiments. The laboratory experiments highlight details of the flow (instability and wave formation) which could be explored in more detail.

In these hydraulic problems the flow is determined by the stratifications in the reservoirs. In general the Bernoulli potentials will not take the same value in both reservoirs. The exchange flow is then composed of a flow satisfying equations (6), in which the Bernoulli potentials are constants, connected to the reservoirs via one or more hydraulic jumps at which the Bernoulli potentials may change. There are thus two steps to solving these fluid flow problems. First, one must determine the appropriate values of the Bernoulli constants and the appropriate branches of the solution for the Bernoulli-potential-conserving section of the flow. Second, one must solve the functional problem represented by equation (7), to determine the values of the fluxes and the structure of the flow.

In this paper we have focused our attention mainly upon the second step. The numerical technique applied can readily be extended to flows with more than three layers. However, the number of controls will in general be greater, adding to the computational difficulty. For most of the reservoir stratifications used in this paper the first step has been straightforward. In all cases, it was required that there be no net energy gain at the jump. However, satisfying this condition is not sufficient to determine the existence of a flow type. It is necessary to solve the functional solution to verify the solution.

Whenever a layer is absent in a reservoir we have assumed that the appropriate branch of the solution is the supercritical flow in which that layer depth tends to zero as $|x| \to \infty$. There are some exceptions to this rule, for example the flow types sketched in figure 10(c) (i, ii) that occur for $y_{1-} > y_{1+}$ with $r_1 = 0.5$. In this paper these exceptions were determined by examining the behaviour of the solutions as the parameter values were varied. Increasing the number of layers will significantly add to the difficulty of this step.

While the theory is presented in general terms, more detailed calculations could be conducted for flows with a net, forced flux through the channel and for more complicated channels, including non-rectangular and having combinations of sills and narrows. A further area that we will investigate is the effect of rotation on the flow. The hydraulic functional formulation is suitable for incorporating this effect when the potential vorticity is uniform in each layer (Gill 1977; Dalziel 1990). An interesting aspect of rotating multi-layer flows is that the different wave modes may be affected in different ways. For the flow through Bab al Mandab, for example, the Rossby radius based on the speed of mode 1 internal waves is significantly larger than the width of the strait (and so rotation would have little effect on this mode), while the Rossby radius for the second wave mode is of the same order as the width of the strait (Pratt *et al.* 1999). Thus the importance of rotation depends on how the flow is controlled.

with the design and construction of the apparatus. We also thank the referees for their many useful suggestions for improving our original manuscript.

Appendix A. Numerical solutions

For the examples given in this paper the channel geometry is described by

$$b(x) = b_m + (1 - b_m)e^{-x^2}, \tag{A 1}$$

The maximum non-dimensional width, b_m, was set equal to 3.5, approximately equal to the ratio of the reservoir width to the constriction width in the laboratory experiments.

For given values of the fluxes and the Bernoulli constants, solutions for the layer thicknesses, y_i, as a function of x were obtained as follows. Given values $y_1(x), y_2(x)$ estimates of $y_1(x + \delta x), y_2(x + \delta x)$ were calculated using a forward difference form of equations (9). These estimates were then used as an initial guess for a numerical procedure to find solutions to equations (6.1) and (6.2) at $x + \delta x$. To ensure that solutions were obtained for the correct branch, the value of δx was varied so that smaller values were used when the gradients of the y_i were large or when a control was approached.

Values of the fluxes and Bernoulli constants (if they are not defined by the reservoir conditions) were obtained by solving a set of coupled nonlinear equations. For flows with m controls the number of equations to be solved is $4m - 1$. These are: the two Bernoulli equations (6.1) and (6.2) at each control, the criticality equation (27) at each control, and the regularity condition (28) at each control except the geometric control. The variables for these equations include y_1, y_2 at each control, and the locations x_v of each of the $m - 1$ virtual controls. The remaining m variables are the unknown flux (one control), two fluxes (two controls) or two fluxes and one Bernoulli constant (three controls).

If one of the virtual controls is located at the geometric control then the four equations (and three variables) corresponding to the virtual control are redundant. These are replaced by a single equation:

$$\frac{\partial \det \boldsymbol{M}}{\partial x} = 0 \quad \text{at} \quad x = 0 \tag{A 2}$$

If the flux in one layer is zero, then the equations to be solved will be modified. For example, the case of a stagnant middle layer is discussed in Smeed (2000).

Appendix B. Determining Bernoulli constants in the channel

The basic state considered in figure 3, type 0, is one in which the stratification is the same in both reservoirs ($y_{1-} = y_{1+} = 0.4$, $y_{2-} = y_{2+} = 0.2$). Here we consider small variations about this basic state. The difference between the height of the upper interface in the right- and left-hand reservoirs is

$$\Delta \text{ Upper} = y_{1+} - y_{1-}. \tag{B 1}$$

The corresponding difference for the lower interface is

$$\Delta \text{ Lower} = y_{1+} + y_{2+} - y_{1-} - y_{2-}. \tag{B 2}$$

In the reservoirs the Bernoulli constants are (noting that $h = 1$) given by

$$H_{1\pm} = ry_{1\pm}, \tag{B 3}$$

$$H_{2\pm} = (1 - r)(y_{1\pm} + y_{2\pm}), \tag{B 4}$$

where $+$ $(-)$ refers to the right- (left-) hand reservoir. Applying the condition that there be no energy gain at a jump, we can now examine the conditions under which each of the flows illustrated in figure 3(b) can occur. The results are illustrated in figure 3(c). Note, however, that the energy conditions presented below are necessary but not sufficient conditions for the flow to occur. The existence of the flow must be verified by solution of the functional equations. Thus, these results are valid only for small departures from the example of type 0 given in figure 3.

A full description of the possible flow states as a function of the full (five-dimensional) parameter space of possible reservoir conditions is beyond the scope of this paper. However, some of the other possible flow types are described at the end of this Appendix. First we consider the flow types illustrated in figure 3.

Type a In this case the upper layer must have the same depth in both reservoirs i.e.

$$\Delta \text{ Upper} = 0. \tag{B 5}$$

So that the energy condition is satisfied, the Bernoulli constant, H_2, is determined by the lesser of H_{2+} and H_{2-}, i.e. type a occurs for Δ Lower < 0 and type a' for Δ Lower > 0.

Type b In this case the lower layer must have the same depth in both reservoirs, i.e.

$$\Delta \text{ Lower} = 0. \tag{B 6}$$

So that the energy condition is satisfied, the Bernoulli constant, H_1, is determined by the greater of H_{1+} and H_{1-}, i.e. type b occurs for Δ Upper < 0 and type b' for Δ Upper > 0.

Type c In this case the sum $H_1 + H_2$ is the same in both reservoirs. When $r = 0.5$ this is equivalent to

$$\Delta \text{ Upper} + \Delta \text{ Lower} = 0. \tag{B 7}$$

The energy condition implies that the Bernoulli constants H_1 and H_2 are set by the reservoir for which $H_2 - H_1$ is the greatest. For $r = 0.5$ this is the right- (left-) hand reservoir when Δ Upper $< (>)0$, giving type $c(c')$.

Type x For type x, H_1 is set by the left-hand reservoir and H_2 is set by the right-hand reservoir; thus the energy conditions require that $H_{1+} < H_{1-}$ and $H_{2+} < H_{2-}$. When $r = 0.5$, this is equivalent to

$$\Delta \text{ Upper} < 0 \quad \text{and} \quad \Delta \text{ Lower} < 0. \tag{B 8}$$

Similarly for type x' the conditions are that

$$\Delta \text{ Lower} > 0 \quad \text{and} \quad \Delta \text{ Upper} > 0. \tag{B 9}$$

Type y In this case H_2 is set by the right-hand reservoir and $H_1 + H_2$ is set by the left-hand reservoir, so that $H_2 = H_{2+}$ and $H_1 = H_{1-} + H_{2-} - H_{2+}$. Thus the energy conditions are $H_2 - H_1 > H_{2-} - H_{1-}$ and $H_1 > H_{1+}$ implying that $H_{2+} > H_{2-}$ and $H_{1+} + H_{2+} < H_{1-} + H_{2-}$. When $r = 0.5$, this is equivalent to

$$\Delta \text{ Upper} + \Delta \text{ Lower} < 0 \quad \text{and} \quad \Delta \text{ Lower} > 0. \tag{B 10}$$

Similarly for type y' the conditions are that

$$\Delta \text{ Upper} + \Delta \text{ Lower} > 0 \quad \text{and} \quad \Delta \text{ Lower} < 0. \tag{B 11}$$

Type z In this case H_1 is determined by the left-hand reservoir and $H_1 + H_2$ is set by the right-hand reservoir, so that $H_1 = H_{1-}$ and $H_1 = H_{1+} + H_{2+} - H_{2-}$. Thus the
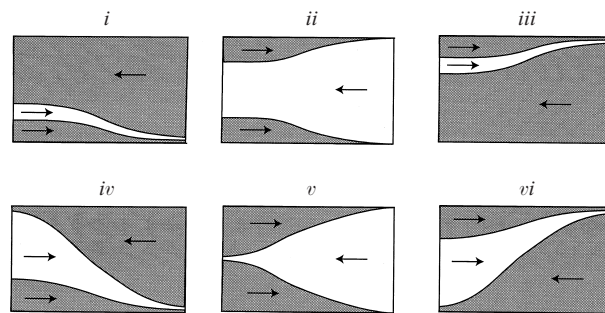
FIGURE 14. (*i–iii*) Examples of flow types with two controls in which there is a region where the flow is subcritical with respect to both modes and another region where the flow is supercritical with respect to both modes, (*iv–vi*): Examples of flow types with three controls.

energy conditions are $H_2 - H_1 > H_{2-} - H_{1-}$ and $H_2 < H_{2+}$ implying that $H_{1+} < H_{1-}$ and $H_{1+} + H_{2+} > H_{1-} + H_{2-}$. When $r = 0.5$, this is equivalent to

$$\Delta \text{ Upper} + \Delta \text{ Lower} > 0 \quad \text{and} \quad \Delta \text{ Upper} < 0 \qquad (\text{B}\,12)$$

Similarly for type z' the conditions are that

$$\Delta \text{ Upper} + \Delta \text{ Lower} < 0 \quad \text{and} \quad \Delta \text{ Upper} > 0. \qquad (\text{B}\,13)$$

Further flow types Reservoir conditions significantly different from the basic state in figure 3 can give rise to different flow types; some examples were discussed in § 5. Six of these other types are illustrated in figure 14.

Types *i–iii* are further examples of flows with two controls, but in these flows both Bernoulli constants are set in the left-hand reservoir. Approaching the right-hand reservoir both modes are supercritical.

Types *iv–vi* are examples of flows with three controls. For these flow types only one of the Bernoulli constants is determined by reservoir conditions (in the left-hand reservoir), the other is determined by the solution of the hydraulic functional. Approaching the right-hand reservoir both modes are supercritical, and approaching the left-hand reservoir one mode is supercritical. Note that type *v* was discussed in § 5.1 (case A, when there was non-zero flux in each of the layers), and also § 5.2 (case B, when $y_{1+} < 0.25$ (for $r = 0.5$)).

REFERENCES

ARMI, L. 1986 The hydraulics of two flowing layers with different densities. *J. Fluid Mech.* **163**, 27–58.

ARMI, L. & FARMER, D. M. 1986 Maximal two-layer exchange through a contraction with barotropic net flow. *J. Fluid Mech.* **164**, 27–51.

ARMI, L. & WILLIAMS, R. 1993 The hydraulics of a stratified fluid flowing through a contraction. *J. Fluid Mech.* **251**, 355–375.

BAINES, P. G. 1987 Upstream blocking and airflow over mountains. *Ann. Rev. Fluid Mech.* **19**, 75–97.

BAINES, P. G. 1988 A general method for determining upstream effects in stratified flow of finite depth over long two-dimensional obstacles. *J. Fluid Mech.* **188**, 1–22.

BAINES, P. G. 1995 *Topographic Effects in Stratified Flows.* Cambridge University Press.

BENJAMIN, T. B. 1981 Steady flows drawn from a stably stratified reservoir. *J. Fluid Mech.* **106**, 245–260.

BOREMANS, M. & GARRETT, C. 1989 The effects of nonrectangular cross section, friction and barotropic fluctuations on exchange through the strait of Gibraltar. *J. Phys. Oceanogr.* **19**, 1543–1557.

Bryden, H. L., Candella, J. & Kinder, T. H. 1994 Exchange through the strait of Gibraltar. *Prog. Oceanogr.* **33**, 201–248.

Bryden, H. L. & Kinder, T. H. 1991 Steady two-layer exchange through the strait of Gibraltar. *Deep-Sea Res.* **38**, 5445–5463.

Dalziel, S. B. 1990 Rotating two-layer sill flows. In *The Physical Oceanography of Sea Straits* (ed. L. J. Pratt), pp. 343–371. Kluwer.

Dalziel, S. B. 1991 Two-layer hydraulics: a functional approach. *J. Fluid Mech.* **223**, 135–163.

Dalziel, S. B. 1992a Maximal exchange in channels with nonrectangular cross-sections. *J. Phys. Oceanogr.* **22**, 1188–1206.

Dalziel, S. B. 1992b Decay of rotating turbulence: some particle tracking experiments. *Appl. Sci. Res.* **49**, 217–244.

Denton, R. F. 1990 Classification of unidirectional three-layer flow over a bump. *J. Hydraulic Res.* **28**, 215–223.

Engqvist, A. 1996 Self-similar multi-layer exchange flow through a contraction. *J. Fluid Mech.* **328**, 49–66.

Farmer, D. M. & Armi, L. 1986 Maximal two-layer exchange over a sill and through the combination of a sill and contraction with barotropic flow. *J. Fluid Mech.* **164**, 53–78.

Farmer, D. M. & Armi, L. 1988 The flow of Mediterranean water through the strait of Gibraltar, *Prog. Oceanogr.* **27**, 1–41.

Gill, A. E. 1977 The hydraulics of rotating channel flow. *J. Fluid Mech.* **80**, 641–671.

Helfrich, K. R. 1995 Time-dependent two-layer exchange flows. *J. Phys. Oceanogr.* **13**, 695–708.

Imberger, J. & Patterson, J. C. 1989 Physical Limnology. *Adv. Appl. Mech.* **27**, 303–475.

Killworth, P. D. 1992 On hydraulic control in a stratified fluid. *J. Fluid Mech.* **237**, 605–626.

Lane-Serff, G. F. & Woodward, M. D. 2000 Internal bores in two-layer exchange flows over sills. *Deep-Sea Res.* I (in press)

Murray, S. P. & Johns, W. 1997 Direct observations of seasonal exchange through the Bab el Mandab strait. *Geophys. Res. Let.* **24**, 2557–2560.

Pratt, L., Johns, W., Murray, S. P. & Katsumata, K. 1999 Hydraulic interpretation of direct velocity measurements in the Bab al Mandab. *J. Phys. Oceanogr.* **29**, 2769–2784.

Pratt, L. J. & Lundberg, P. A. 1991 Hydraulics of rotating strait and sill flows. *Ann. Rev. Fluid Mech.* **23**, 81–106.

Smeed, D. 1997 Seasonal variation of the flow in the strait of Bab al Mandab. *Oceanologica Acta*, **20**, 773–781.

Smeed, D. A. 2000 Hydraulic control of three-layer exchange flows: application to the Bab al Mandab. *J. Phys. Oceanogr.* (in press).

Wood, I. R. 1970 A lock exchange flow. *J. Fluid Mech.* **42**, 671–687.